

SinMPI: Novel View Synthesis from a Single Image with Expanded Multiplane Images

Guo Pu
guopu@pku.edu.cn
Wangxuan Institute of Computer
Technology, Peking University
Beijing, China

Peng-Shuai Wang
wangps@hotmail.com
Wangxuan Institute of Computer
Technology, Peking University
Beijing, China

Zhouhui Lian*
lianzhouhui@pku.edu.cn
Wangxuan Institute of Computer
Technology, Peking University
Beijing, China

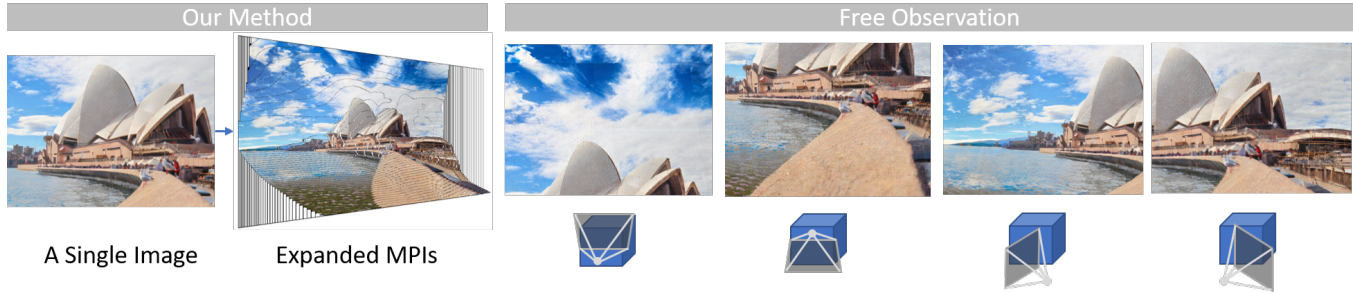


Figure 1: With only a single image as input, our method constructs its expanded multiplane image, allowing free observation from a large range of perspectives.

ABSTRACT

Single-image novel view synthesis is a challenging and ongoing problem that aims to generate an infinite number of consistent views from a single input image. Although significant efforts have been made to advance the quality of generated novel views, less attention has been paid to the expansion of the underlying scene representation, which is crucial to the generation of realistic novel view images. This paper proposes SinMPI, a novel method that uses an expanded multiplane image (MPI) as the 3D scene representation to significantly expand the perspective range of MPI and generate high-quality novel views from a large multiplane space. The key idea of our method is to use Stable Diffusion [Rombach et al. 2021] to generate out-of-view contents, project all scene contents into an expanded multiplane image according to depths predicted by monocular depth estimators, and then optimize the multiplane image under the supervision of pseudo multi-view data generated by a depth-aware warping and inpainting module. Both qualitative and quantitative experiments have been conducted to validate the superiority of our method to the state of the art. Our code and data are available at <https://github.com/TrickyGo/SinMPI>.

*Corresponding author

Permission to make digital or hard copies of all or part of this work for personal or classroom use is granted without fee provided that copies are not made or distributed for profit or commercial advantage and that copies bear this notice and the full citation on the first page. Copyrights for components of this work owned by others than the author(s) must be honored. Abstracting with credit is permitted. To copy otherwise, or republish, to post on servers or to redistribute to lists, requires prior specific permission and/or a fee. Request permissions from permissions@acm.org.

SA Conference Papers '23, December 12–15, 2023, Sydney, NSW, Australia
© 2023 Copyright held by the owner/author(s). Publication rights licensed to ACM.
ACM ISBN 979-8-4007-0315-7/23/12...\$15.00
<https://doi.org/10.1145/3610548.3618155>

CCS CONCEPTS

• **Computing methodologies** → **Computer graphics; Rendering.**

KEYWORDS

Novel view synthesis, Multiplane images, Diffusion models

ACM Reference Format:

Guo Pu, Peng-Shuai Wang, and Zhouhui Lian. 2023. SinMPI: Novel View Synthesis from a Single Image with Expanded Multiplane Images. In *SIGGRAPH Asia 2023 Conference Papers (SA Conference Papers '23)*, December 12–15, 2023, Sydney, NSW, Australia. ACM, New York, NY, USA, 10 pages. <https://doi.org/10.1145/3610548.3618155>

1 INTRODUCTION

Single-image novel view synthesis substantially narrows the gap between 2D images and 3D experiences, empowering the generation of an infinite number of views from a single input image. While the geometry of the input image can be obtained by monocular depth estimators (e.g., DPT [Ranftl et al. 2021]), the major challenge lies in inferring the occluded content and reconstructing the missing geometry with exceedingly under-constrained 3D conditions provided by the single input image.

NeRF [Mildenhall et al. 2021] and its following works have demonstrated their ability to render high-quality images. However, optimizing the continuous fields of NeRF requires sufficient multi-view inputs. Due to insufficient input information, the state-of-the-art single-image NeRF-based method SinNeRF [Xu et al. 2022] produces novel views with blurry and flickering artifacts.

With the limited information provided by a single perspective, modeling the 3D scene using discrete multi-plane representation is more efficient than continuous radiance field representations.

MPI-based methods [Shade et al. 1998; Szeliski and Golland 1999; Zhou et al. 2018] represent the 3D scene using multiple planes in a perspective frustum, possess higher efficiency and require lower computational cost compared to methods (e.g., NeRF) using continuous 3D representations at the expense of continuous expression ability. Benefiting from the efficiency of MPIs, AdaMPI [Han et al. 2022] achieves state-of-the-art performance in single-image novel-view synthesis for images in the wild. However, MPI-based methods are constrained in their modeling space to the original camera frustum. Moreover, their rendered results may be plagued by depth discretization artifacts and repeated texture artifacts, which hinder their applications in practical use.

To overcome these limitations, we propose SinMPI, which leverages an expanded, learnable MPI with a wider view range to represent an extended scene from a single image. Compared with previous MPI-based methods, our approach significantly enhances the capacity of modeling the 3D scene and permits a larger range of camera movements beyond the boundaries of the input image. Unlike previous MPI-based methods, which attempt to predict occluded geometry information in space using image generators which generate low-quality texture extensions, we leverage an MPI as a volumetric scene representation and fill in missing geometry supervised by pseudo-multi-view images. A key difference is that we represent our MPI as learnable parameters that are directly optimized through volume rendering, considering the expanded 3D scene is more complex and challenging to predict in a single pass. In this manner, our approach not only yields an expanded multi-plane representation that allows free observation and fast, 3D-consistent novel view synthesis, but also effectively alleviates the depth discretization artifacts and the repeated texture artifacts through volume rendering. Experimental results demonstrate that our method not only achieves the best single-image novel view synthesis results in real-world scenarios, but also possesses remarkable scene extension capabilities.

In summary, the major contributions of this paper are as follows:

1. We introduce SinMPI, a novel single-image view synthesis method that constructs an expanded multiplane image from a single input view, enabling unrestricted observations and fast, 3D-consistent novel view synthesis. Our approach significantly extends the capacity of original MPI-based methods and supports a wider range of camera movements.
2. We leverage an MPI as a volumetric scene representation, which improves the accuracy for fitting missing geometry information and alleviates the depth discretization artifacts and the repeated texture artifacts caused by previous MPI predictors [Han et al. 2022].
3. We extensively evaluate our approach on multiple datasets, including the real-world LLFF dataset, the NeRF synthetic dataset, the DTU dataset, and the COCO dataset. Our method achieves state-of-the-art render quality on single-image novel view synthesis.

2 RELATED WORK

2.1 Single-image Novel View Synthesis

There exist several methods that address the single-image novel view synthesis task without relying on explicit 3D representation for the entire scene, such as DISN [Xu et al. 2019] and Learning-ToRecover [Yin et al. 2021]. SynSin [Wiles et al. 2020] projected the

input view’s point cloud to estimate new points and generate target views through a refinement network. Infinite-Nature [Liu et al. 2021] and Infinite-Nature-Zero [Li et al. 2022] generated perpetual views of natural scenes by using a differentiable mesh renderer and a GAN [Goodfellow et al. 2020] to synthesize novel views. 4D-RGBD-Light Field [Srinivasan et al. 2017] synthesized a light field from an image. Pixelsynth [Rockwell et al. 2021] used point cloud as an intermediate representation and then predicted novel views with CNN decoders. 3DiM [Watson et al. 2022] proposed a geometry-free pose-conditional image-to-image diffusion model.

However, these methods did not employ explicit 3D representations for entire scenes, which limits the 3D view consistency of the generated views and produces flickers and blurs in the synthesized results, especially in occluded regions. In contrast, our method ensures multi-view consistency using a fixed MPI for the entire scene.

2.2 NeRF-based Methods

NeRF [Mildenhall et al. 2021] and its variants have received significant attention in novel view synthesis. However, the original NeRF required at least 100 posed views for input, which was both inconvenient and inaccessible for practical applications. To overcome this challenge, several NeRF-based methods were proposed to generate novel views based on fewer input images, including PixelNerf [Yu et al. 2021], DietNeRF [Jain et al. 2021], Pix2nerf [Cai et al. 2022], PortraitNeRF [Gao et al. 2020], ViTNeRF [Lin et al. 2023], NerfDiff [Gu et al. 2023] and Nerdi [Deng et al. 2023]. For scene-level modeling, SinNeRF [Xu et al. 2022] is the state-of-the-art NeRF-based method for single-image novel view synthesis.

The advantages of NeRF lie in its ability to simultaneously model diffuse and specular color in multi-view images. However, inferring a light field from a single image input is challenging for NeRF. The difficulty of optimizing NeRF from a single input view hampers the ability of NeRF-based methods to generate photo-realistic results. In contrast, MPI, as a diffuse volumetric scene representation, is more efficient and sufficient for tasks where light field information is not required. Nevertheless, the potential of NeRF in modeling view-dependent effects for this task is also worth exploring.

2.3 Layer-based Methods

Layer-based methods represent a 3D scene using discrete layers, resulting in higher efficiency and lower computational cost compared to continuous 3D representations like NeRF. Layer-based methods, such as 3D-photography [Shih et al. 2020] and SLIDE [Jampani et al. 2021], can produce high-quality synthesis results from a single input image.

As a discrete diffuse volumetric scene representation, MPI-based methods [Shade et al. 1998; Szeliski and Golland 1999; Zhou et al. 2018] were proposed to represent the scene using multiple planes in a perspective frustum. Following multi-view MPI-based works [Srinivasan et al. 2019; Wizarawongsa et al. 2021] improved the MPIs render quality. Srinivasan et al. [2019] proposed a two-step MPI prediction procedure to alleviate issues of depth discretization artifacts and repeated texture artifacts that appear in MPIs rendering results. NeX [Wizarawongsa et al. 2021] extended MPIs for non-Lambertian material and was able to handle view-dependent effects effectively. DeepView [Flynn et al. 2019] incorporated occlusion

reasoning to generate an MPI from a set of sparse camera viewpoints. For single-image novel view synthesis, following MPI-based methods (SVMPI [Tucker and Snavely 2020], VMPI [Li and Kalantari 2020], MINE [Li et al. 2021], GMPI [Zhao et al. 2022], and AdaMPI [Han et al. 2022]) trained convolutional image generators to predict missing occluded geometry in the space. However, these methods heavily rely on large-scale datasets to train MPI predictors; thus, the MPI prediction quality is highly constrained by the training data and can hardly adapt to new manifolds, such as synthetic object-centric scenes in Fig. 5.

The typical MPIs renderer only models a frustum range, resulting in a limited view field that hinders the practical application. To address this issue, we propose a novel method that uses larger planes in space to expand the view range. Additionally, MPI-based methods' rendering results often suffer from depth discretization artifacts and repeated texture artifacts. We alleviate these issues by optimizing an MPI through volume rendering.

3 METHOD

In this section, we present the details of our SinMPI, which expands the perspective range of an MPI and generates high-quality 3D-consistent novel views. The key idea is to generate out-of-view contents via Stable Diffusion [Rombach et al. 2021], project them into a multiplane image, then optimize the MPI under the supervision of pseudo-multi-view images generated by a depth-aware warping and inpainting module. Fig. 2 illustrates the pipeline of our method, and additional details are presented in the following subsections.

3.1 Continuous Outpainting Module

We utilize Stable Diffusion [Rombach et al. 2021] to perform continuous extrapolation of user-provided reference images for scene expansion. The inpainting model based on Stable Diffusion, leverages semantic masks as a conditioning input, and the conditional latent diffusion model is trained by minimizing:

$$L_{LDM} := \mathbb{E}_{\epsilon(x), y, \epsilon \sim \mathcal{N}(0,1), t} [\|\epsilon - \epsilon_{\theta}(z_t, t, m)\|_2^2], \quad (1)$$

where $t = 1, 2, \dots, T$ denotes the time step, z_t is the noisy version of the latent vector z of input x , m represents the mask, ϵ is the noise schedule, and ϵ_{θ} denotes the time-conditioned UNet, respectively.

For unposed single images, to maintain consistency with the input view's depth range, we estimate the depth of the reference image using a state-of-the-art depth estimator, DPT [Ranftl et al. 2021], both before and after the outpainting process. Our depth alignment is a linear scale and shift of the outpainted monocular depth which preserves the depth range of the original areas. We align the depth of the original region accordingly, resulting in the reference image I_{ref} , its depth D_{ref} , the expanded image I_{exp} , and its depth D_{exp} . Importantly, we ensure that the geometry in the original view remains in the same depth range and the pre-defined camera trajectories are unchanged.

3.2 Depth-aware Inpainting Module

To reconstruct a complete 3D scene from the outpainted image and its aligned depth, we need to infer the occluded content. We start by treating the pixels of the reference view, along with their depth values, as a point cloud in space. We then use depth-warp [Huang

et al. 2021] to warp the original image to novel viewpoints, which involves computing:

$$p_j = \hat{K}T(K^{-1}D_i p_i), \quad (2)$$

where p denotes the pixel point, i , and j denote the indices of the source and target views, respectively, T is the camera extrinsic, D represents the depth, and K and \hat{K} denote the source and target camera intrinsics, respectively.

To generate projected views, we render the warped point cloud with the Painter's Algorithm [Newell et al. 1972] to choose points nearest to the camera. This process creates novel views with missing areas that require proper inpainting to obtain a complete novel view.

For inpainting, we draw inspiration from 3D-photography [Shih et al. 2020] and AdaMPI [Han et al. 2022] and use a depth-aware inpainter based on Edge-connect [Nazeri et al. 2019] which is constructed by an edge inpainter, followed by a depth inpainter and an image inpainter. The inpainter is pretrained on the Places2 dataset [Zhou et al. 2017a] and then we deploy a per-scene fine-tuning on the input image I_{exp} .

To fine-tune the inpainter on a single image, we first warp the image I_{exp} to a novel view $T * I_{exp}$ according to a sampled camera T . We then inpaint the warped image to obtain the inpainted image I_{inp} . Since there is no ground truth available for I_{inp} , we utilize deep features extracted from specific layers of a pre-trained VGG network for texture matching at the feature/patch level. The perceptual loss is defined as:

$$L_{per}(I_{inp}, I_{exp}) = \frac{1}{N_l} \sum_{x=1}^{W_l} \sum_{y=1}^{H_l} \sum_{z=1}^{C_l} \|\phi_l(I_{inp})_{x,y,z} - \phi_l(I_{exp})_{x,y,z}\|_1, \quad (3)$$

where ϕ_l denotes the output feature of the layer l of the VGG19 network, N_l equals $W_l H_l C_l$, and W_l , H_l and C_l represent the spatial width, height, and depth of the feature ϕ_l , respectively.

In addition to the VGG-based perceptual loss, we also incorporate the features from a vision transformer to calculate the ViT loss:

$$L_{vit}(I_{inp}, I_{exp}) = \|f_{vit}(I_{inp}) - f_{vit}(I_{exp})\|^2, \quad (4)$$

where f_{vit} denotes the feature extracted by DINO-ViT [Caron et al. 2021] pre-trained on the ImageNet [Deng et al. 2009] dataset.

Next, we warp the image $T * I_{exp}$ back by computing $T^{-1} * T * I_{exp}$ and then obtain the inpainted warp-back image I_{inp}^{WB} . The warp-back depth is also inpainted to get D_{inp}^{WB} . To ensure that the reconstructed image and depth are accurate, we apply the reconstruction loss, along with the VGG/ViT feature/patch level losses, to the reconstructed image. The reconstruction loss is defined as:

$$L_{rec}(I_{inp}^{WB}, I_{exp}) = \|I_{inp}^{WB} - I_{exp}\|_1. \quad (5)$$

To enforce depth consistency, we apply the depth loss to the inpainted depth:

$$L_{depth}(D_{inp}^{WB}, D_{exp}) = \|D_{inp}^{WB} - D_{exp}\|_1, \quad (6)$$

where D_{exp} and D_{inp}^{WB} represent the depth map of the expanded image and the inpainted warp-back depth map, respectively.

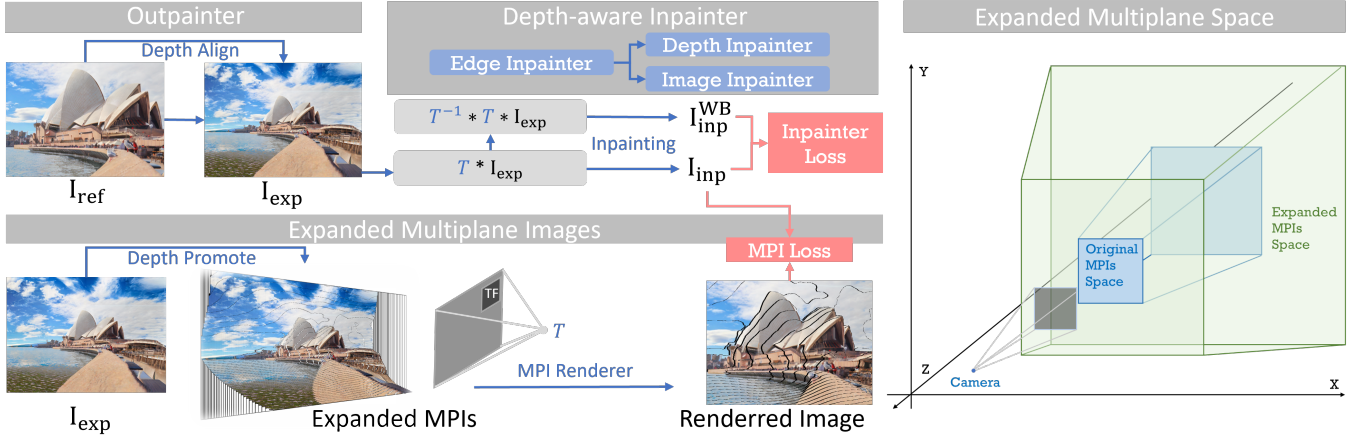


Figure 2: The pipeline of our SinMPI consists of three major components: a continuous outpainter, a depth-aware inpainter, and an expanded MPI. We first extrapolate out-of-scene contents, infer the scene’s 3D geometry and occluded contents, and finally convert the scene into a multiplane space. Note that trainable filters (TF) are used to aggregate local rays. On the right, we show our expanded multiplane space. To enable the construction of larger 3D spaces, we employ larger planes within a larger frustum (green) than the camera frustum (blue) in our expanded MPI space. This approach allows for larger camera view ranges, including larger rotation angles than those supported by existing MPI-based methods.

The total loss for finetuning the inpainter is:

$$\begin{aligned}
 L_{\text{inpainter}}(I_{\text{inp}}, D_{\text{inp}}, I_{\text{inp}}^{\text{WB}}, D_{\text{inp}}^{\text{WB}}, I_{\text{exp}}, D_{\text{exp}}) = & \\
 \lambda_{\text{rec}} L_{\text{rec}}(I_{\text{inp}}^{\text{WB}}, I_{\text{exp}}) + \lambda_{\text{depth}} L_{\text{depth}}(D_{\text{inp}}^{\text{WB}}, D_{\text{exp}}) + & \quad (7) \\
 \lambda_{\text{per}} L_{\text{per}}(I_{\text{inp}}^{\text{WB}}, I_{\text{exp}}) + \lambda_{\text{vit}} L_{\text{vit}}(I_{\text{inp}}^{\text{WB}}, I_{\text{exp}}) + & \\
 \lambda_{\text{per}} L_{\text{per}}(I_{\text{inp}}, I_{\text{exp}}) + \lambda_{\text{vit}} L_{\text{vit}}(I_{\text{inp}}, I_{\text{exp}}), &
 \end{aligned}$$

where λ_{rec} , λ_{depth} , λ_{per} , and λ_{vit} denote the loss weights. We experimentally found that finetuning the inpainting model for around 100 iterations per view strikes a good balance between underfitting and overfitting.

Using our finetuned depth-aware warping and inpainting module, we generate pseudo-multi-view data by first warping the source point to target views via depth warping and then inpainting the holes of warped images from different perspectives of the 3D scene. Note that the generated pseudo-novel views may contain certain pixels that are not fully 3D-consistent due to the lack of explicit 3D geometry information in the inpainted areas. To address this issue, we use pseudo-novel views to optimize a single MPI, thereby enabling the creation of a complete and static 3D representation.

3.3 Expanded MPI

As information from a single view is inadequate to fully capture a 3D scene, we employ discrete multiplane representations, which are efficient and feasible for the task of synthesizing novel views from a single image. Due to the substantially reduced computational costs compared to continuous representations, our method can efficiently construct large 3D spaces and generate photo-realistic novel views that span a large view range. To accomplish this, we first project all contents onto our expanded multiplane image and then optimize the multiplane image using previously-generated pseudo-multi-view images as supervision.

3.3.1 MPI Initialization. Since the points of the original view provide the ground-truth information in the 3D space for single-image novel view synthesis, they should remain fixed. Therefore, we segment the original image according to depth and project it onto multiple planes evenly distributed along the depth. Each plane stores only a small range of the depth space and has its initialized contents frozen in the following procedures. Our expanded MPI contains $P * H * W * 4$ parameters, where P denotes the number of planes, $H * W$ represents the size of a plane, and 4 is the channel number of a point in a plane, which stores the point’s RGB values and density.

3.3.2 MPI Renderer. The original method using MPIs represents the 3D scene as a series of parallel planes in a view frustum. The plane homography transformation [Hartley and Zisserman 2003] is defined by:

$$[x_i, y_i, 1]^T \sim K(R - \frac{tn^T}{d_k})K^{-1} [x_j, y_j, 1]^T, \quad (8)$$

where $n = [0, 0, 1]^T$ is the plane normal, d_k is the depth of the plane k , x and y denote the coordinates of a pixel in the target view j or source view i , respectively, K denotes the camera intrinsics, and R and t are the rotation and translation matrices, respectively.

The layers of our MPI are distributed evenly along the z -axis of the entire 3D space. We render the target view through volume rendering using the following equations:

$$I = \sum_{i=1}^N T_i (1 - \exp(-\sigma_{d_i} \delta_{d_i})) c_{d_i}, \quad (9)$$

$$T_i = \exp(-\sum_{j=1}^{i-1} (-\sigma_{d_j} \delta_{d_j})), \quad (10)$$

where T denotes the accumulated transmittance starting from the first plane, c denotes the RGB value, and σ represents the density.

Each plane i is considered as a bin along the depth d , and δ is the distance between every two planes, which is a constant in our case due to the even distribution of planes along the depth.

The original method using MPIs simply represents the 3D scene in a view frustum. Once the camera rotates or translates to a certain amount, it can easily exceed the field of the original MPIs' view range. Current MPI-based methods [Han et al. 2022; Li et al. 2021] typically use border pixel extension for out-of-scene contents which generates unnatural textures. This inherent limitation makes the MPIs representation less applicable to real-world scenarios with significant camera movement.

In order to endow MPIs with a wider modeling space, we propose to use larger planes for the view frustum with an increased view angle of θ , while maintaining the camera's original field of view (see the right side of Fig. 2). The relationship between the increased frustum angle and the expanded plane size is defined by: $\frac{w*a}{2f} = \tan(\frac{\theta}{2})$, where w represents the length of the long plane border, a denotes the expansion factor, f is the focal length of the camera, and θ is the view angle range, respectively. During the testing phase, we perform homography transformation on the expanded MPI and only apply volume rendering to the parameters within the camera's field of view instead of all the planes.

3.3.3 Local Rays Aggregation. Unlike existing MPI-based methods that predict MPI through convolutional image decoders, we directly optimize the MPI itself. This novel approach allows for improved optimization efficiency and faster convergence rates since the optimization of each ray is independent. Due to the dense nature of the point cloud representation and the limitation of the inpainting module, our created pseudo views are sharp and prone to noise points as well as flickering artifacts. Alleviating these artifacts requires patch-level supervision.

To facilitate interaction among local rays and create smooth rendered images, we introduce a convolutional filter layer after the MPI renderer to enable sharing of information within local patches and facilitate faster optimization. Specifically, we use a trainable bilateral filter [Tomasi and Manduchi 1998] to aggregate local rays by weighing the influence of neighboring rays based on their intensities and locations. For an MPI rendered image I_{mpi} , we perform the following discrete filter operation:

$$\hat{I}_{mpi}(p) = \frac{1}{W_p} \sum_{q \in S} G_{\delta_s}(\|p - q\|) G_{\delta_r}(\|I_{mpi}(p) - I_{mpi}(q)\|) I_{mpi}(q), \quad (11)$$

with the normalization factor:

$$W_p = \sum_{q \in S} G_{\delta_s}(\|p - q\|) G_{\delta_r}(\|I_{mpi}(p) - I_{mpi}(q)\|), \quad (12)$$

where \hat{I}_{mpi} is the filtered image, p is the pixel index, q is the index in patch S , G_{δ_s} is the learnable Gaussian kernel, G_{δ_r} is the pixel difference kernel, respectively.

To weigh the intensity difference between the center pixel and other pixels, the pixel difference kernel G_{δ_r} is calculated as:

$$G_{\delta_r}(\|I_{mpi}(p) - I_{mpi}(q)\|) = e^{-\frac{\|I_{mpi}(i,j) - I_{mpi}(m,n)\|^2}{2\sigma^2}}, \quad (13)$$

where i and j are the center indices in the patch, m and n are the pixel coordinates in the center index of a patch, and σ is the kernel width, respectively.

To weigh the location difference between the center pixel and other pixels, the learnable Gaussian kernel G_{δ_s} is initialized as:

$$G_{\delta_s}(\|p - q\|) = e^{-\frac{(i-m)^2 + (j-n)^2}{2\sigma^2}}. \quad (14)$$

To make the filtered image smoother without sacrificing quality and reduce the blurry effects of the Gaussian kernel, we make G_{δ_s} trainable as a convolution weight, thereby making the aggregation layer adaptive.

3.3.4 MPI Optimization. As our expanded MPI is specifically designed for single-scene novel view synthesis, we choose to construct them as learnable parameters instead of using an MPI predictor, such as those in [Han et al. 2022; Li et al. 2021]. We found that training large-scale predictors to predict our expanded MPI is both unnecessary and computationally unreasonable.

We optimize the MPI supervised by pseudo-novel-view data created using our depth-aware warping and inpainting module. The full loss function consists of the pixel loss and the feature loss:

$$L_{MPI}(\hat{I}_{mpi}, I_{inp}) = \lambda_{rec} L_{rec}(\hat{I}_{mpi}, I_{inp}) + \lambda_{per} L_{per}(\hat{I}_{mpi}, I_{inp}) + \lambda_{vit} L_{vit}(\hat{I}_{mpi}, I_{inp}), \quad (15)$$

where the λ s are the loss weights.

4 EXPERIMENTS

In this section, we present results that demonstrate the expanded view range and diverse applications of our method. We then conduct a comprehensive quality comparison with state-of-the-art methods to evaluate the performance of SinMPI. In addition, we provide deeper insights into our approach through an ablation study that dissects the contributions of different components in our pipeline.

For more details of our continuous outpainting procedure, implementation specifics, DTU dataset evaluations and efficiency comparisons, please refer to the supplemental material.

4.1 Applications

Our method performs high-quality 3D-consistent novel-view synthesis from a single image. Fig. 7 shows novel views of various expanded scenes generated by our method.

Furthermore, our method can integrate seamlessly with image editing approaches, enabling users to edit 3D scenes. Fig. 3 shows the capabilities of SinMPI, which can synthesize novel views of a street scene and alter its surroundings based on Stable Diffusion's [Rombach et al. 2021] various outpainting outputs.

For all synthesis results presented in the figures, we recommend zooming in for a more detailed inspection. We also highly recommend viewing the supplemental video for a comprehensive 3D-aware inspection that provides a better understanding of the spatial relationships and geometry of the synthesized scenes.

4.2 Expanded View Range

Our scene extrapolating pipeline significantly expands the scene capacity of the original method that adopts MPIs. We show the

differences between ours with the expanded scene and the state-of-the-art MPI-based method AdaMPI [Han et al. 2022] in Fig. 6. Our method generates more photo-realistic results, especially on unseen surrounding regions. Our MPI expansion strategy can be readily applied to any MPI-based method and pushes the bounds of the MPI-based approach’s scene capacity. Nevertheless, due to the high computational cost, our scene-expanding pipeline currently cannot be integrated with other existing approaches to synthesize novel views with the same resolution as our method.

4.3 Comparison with Previous Methods

4.3.1 Baselines. We conduct a comprehensive comparison of SinMPI to several state-of-the-art methods for single-image novel view synthesis, including SinNeRF [Xu et al. 2022] DietNeRF [Jain et al. 2021], PixelNeRF [Yu et al. 2021] and DS-NeRF [Deng et al. 2022], and the state-of-the-art MPI-based single-image novel view synthesis method AdaMPI [Han et al. 2022]. AdaMPI uses a pre-trained model on large datasets (e.g., COCO [Caesar et al. 2018]) for scene prediction, while SinMPI is a per-scene modeling method akin to 3D reconstruction approaches like NeRF, where we train on individual images (scenes) for evaluating novel view renderings.

Comparing these baselines, we observe that AdaMPI produces higher-quality in-fov view synthesis results but SinNeRF’s synthesis results possess a larger view range. However, SinMPI can synthesize novel views with both higher quality and a larger view range.

In our qualitative demonstrations, we mainly compare our method with SinNeRF [Xu et al. 2022] and AdaMPI [Han et al. 2022], since these methods have demonstrated their superiority over other methods in the task of single-image novel view synthesis. Therefore, we omit the demonstrations of other methods’ results and only report their quantitative scores for completeness.

4.3.2 Datasets. We compare rendering quality on the Local Light Field Fusion (LLFF) dataset [Mildenhall et al. 2019], the NeRF synthetic dataset [Mildenhall et al. 2021], and the DTU dataset [Jensen et al. 2014]. These three datasets contain multi-view data that can be used for evaluating both image quality and 3-D consistency. We also compare the performance of different methods by using images contained in COCO [Caesar et al. 2018] and ADE20K [Zhou et al. 2017b]. Note that these two datasets simply consist of individual images without ground-truth multi-view data so only qualitative comparisons are available.

4.3.3 Evaluation Protocol. To conduct a fair comparison, for all methods including ours, the resolutions of input images are identical and their depths are estimated using the same pre-trained multi-view model. Following SinNeRF [Xu et al. 2022], the depth maps used for the NeRF synthetic dataset and LLFF dataset are predicted by a pre-trained NeRF and the depth maps used for the DTU dataset are predicted by MVSNet. Notice that all the methods can generate novel views with the monocular predicted depth such as the DPT [Ranftl et al. 2021] predicted depth, but in order to faithfully evaluate the generated views the depth should match the scene scale so that the generated views are aligned with the corresponding ground-truth images.

For all quantitative comparisons with other methods, we do not use Stable Diffusion to outpaint the input image to keep inputs for

Table 1: Quantitative comparison of our method against other state-of-the-art methods evaluated on the LLFF dataset.

Method	Room			Flower		
	SSIM↑	PSNR↑	LPIPS↓	SSIM↑	PSNR↑	LPIPS↓
DS-NeRF	0.65	17.44	0.40	0.41	16.92	0.39
DietNeRF	0.49	15.77	0.75	0.20	13.35	0.75
PixelNeRF	0.41	12.88	0.76	0.19	13.20	0.63
SinNeRF	0.67	18.85	0.38	0.41	17.20	0.37
AdaMPI	0.62	13.45	0.51	0.32	12.70	0.53
Ours	0.70	17.20	0.34	0.38	15.57	0.38

all methods the same. We would like to emphasize that although our method generates more photorealistic extrapolated scenes when using outpainted images as input, the matching scores with ground-truth novel views are reduced compared to those using original images, indicating a greater mismatch with the ground-truth multi-view images introduced by the outpainting process, including scene scale mismatch due to monocular depth re-estimation and randomness in the outpainted areas.

4.3.4 Evaluation Metrics. We assess performance using some commonly used image quality evaluation metrics, including SSIM, PSNR, and LPIPS [Zhang et al. 2018].

4.4 Evaluation on the LLFF Dataset

4.4.1 Qualitative Comparison. The LLFF dataset consists of real-world forward-facing scenes. For each scene, we randomly choose a posed view as the reference view and the remaining views are used as the test set.

As shown in the top two rows of Fig. 4, our method produces more photorealistic results with higher resolution compared to SinNeRF, due to the layer-based representation’s greater computational efficiency and ability to faithfully preserve the original image’s resolution and textures. Our per-scene optimization and volume rendering strategy empowers our method to surpass the performance of AdaMPI. In the last two rows of Fig. 4, we illustrate that SinMPI performs significantly better than previous methods when equipped with our scene extrapolating strategy, providing a much broader view range.

4.4.2 Quantitative Comparison. Table 1 compares the quantitative results of three different methods evaluated on the LLFF dataset. We observe that our method performs better than AdaMPI on the Flower and Room subsets and outperforms SinNeRF on the Room subset. It should be pointed out that the Flower subset’s multi-view data contains up to 19% out-of-view pixels, but MPI-based methods (i.e., AdaMPI and Ours w/o outpainting) cannot generate out-of-view pixels, which negatively impacts the evaluation scores. Nevertheless, the high-quality synthesis results produced by our method are easily noticeable in the supplemental video. While it is evident from our rendered results that our method produces sharper outputs which match the ground truth better compared to SinNeRF, SinNeRF has the best PSNR score, mainly due to the fact that blurry or repetitive patterns of SinNeRF react positively for the PSNR score. Our method achieves better scores against AdaMPI, which indicates the best generated texture quality of our method.

Table 2: Quantitative comparison of our method against other state-of-the-art methods on the NeRF Synthetic dataset.

Method	Lego			Hotdog		
	SSIM \uparrow	PSNR \uparrow	LPIPS \downarrow	SSIM \uparrow	PSNR \uparrow	LPIPS \downarrow
DS-NeRF	0.77	16.62	0.17	0.67	14.16	0.29
DietNeRF	0.72	15.07	0.21	0.69	16.28	0.26
PixelNeRF	0.72	14.25	0.22	0.71	16.67	0.24
SinNeRF	0.82	20.97	0.09	0.77	19.78	0.17
AdaMPI	0.82	19.20	0.20	0.82	18.40	0.19
Ours	0.87	22.99	0.09	0.84	22.29	0.12

4.5 Evaluation on the NeRF Synthetic Dataset

4.5.1 Qualitative Comparison. The NeRF synthetic dataset contains images focusing on delicate objects with large camera rotations. For each scene of this dataset, we randomly choose a posed image as the reference view. To align with SinNeRF [Xu et al. 2022], the test set consists of 60 posed images that are rendered in Blender by rotating the reference view’s camera pose around y-axis in a degree range of $[-30, 30]$.

Fig. 5 shows the qualitative comparison of SinNeRF and our SinMPI evaluated on the NeRF synthetic dataset. SinNeRF’s results exhibit more noise due to MLP underfitting from limited one-view information. On the other hand, AdaMPI’s results are prone to heavy depth discretization artifacts and repeated texture artifacts caused by its MPI predictors. Our method, in contrast, generates novel-view images with high-quality geometry. We achieve this by leveraging MPIs as a volumetric scene representation, which enhances the accuracy of fitting missing geometry information and mitigates depth discretization artifacts and repeated texture artifacts.

4.5.2 Quantitative Comparison. We also quantitatively compare the performance of SinNeRF and our method on the NeRF synthetic dataset. Table 2 presents the comparison results, which demonstrate that our approach outperforms SinNeRF in synthesizing novel-view images with better structures and textures.

4.6 Ablation Study

4.6.1 Inpainting Module. While Stable Diffusion [Rombach et al. 2021] is effective for outpainting in our approach, it is not 3D-aware, which can lead to unstable and flickering contents when the camera moves. Additionally, Stable Diffusion struggles to inpaint highly irregular missing areas due to its pre-training routine. Furthermore, finetuning the pretrained Stable Diffusion model on a single image is not feasible in our case. Fig. 8 presents a comparison of different inpainting methods. Our approach achieves the best results. In contrast, Stable Diffusion [Rombach et al. 2021] struggles to inpaint complex missing areas in this task.

4.6.2 MPI Module. Table 3 demonstrates that our method achieves higher image quality in the synthesis results based on MPI compared to our pseudo-novel-view data generated by the depth-aware inpainter. Our qualitative results further support the effectiveness of MPI in stabilizing inpainted areas that lack explicit 3D geometry, resulting in more realistic outcomes with improved 3D consistency.

In Fig. 9, we show the qualitative ablation study conducted to investigate our method. Starting with the reference image and its

Table 3: The ablation study on DTU scan 84. PF, PV, and TF refer to per-scene finetuning, pseudo-views, and trainable filters, respectively.

Method	DTU Scan-84			LLFF Room		
	SSIM \uparrow	PSNR \uparrow	LPIPS \downarrow	SSIM \uparrow	PSNR \uparrow	LPIPS \downarrow
AdaMPI	0.70	19.03	0.39	0.68	16.04	0.34
w/o PF	0.67	17.96	0.41	0.66	16.40	0.37
Our PV	0.69	18.11	0.39	0.67	16.86	0.34
w/o TF	0.75	18.23	0.39	0.68	16.60	0.35
Ours	0.76	18.72	0.38	0.70	17.20	0.34

estimated depth from DTU scan 84, we employ point cloud perspective warp to render the novel view together with depth information. Black holes/areas in the rendered image indicate missing geometry and our depth-aware inpainter completes both the image and the depth to generate pseudo views. Guided by these inpainted pseudo views, we fit the expanded MPI to obtain the final results. Our finetune strategy improves the quality of inpainted textures by resolving issues such as misalignment with the pretrained routine and ignoring small missing areas in the input data. Our trainable filter effectively removes noisy points in the pseudo views caused by points projection and generates smoother views and accelerates the optimization process by sharing information between rays.

Table 3 presents the ablation study, where we evaluate the performance of our method without different major components to assess the impact of these design choices on the final metrics.

5 LIMITATIONS

As a common issue for single-image novel view synthesis methods, our SinMPI heavily relies on the accuracy of the depth estimator and cannot fix depth estimation errors. Additionally, similar to other MPI-based approaches, SinMPI performs poorly on slanted surfaces. Furthermore, the inpainter used in SinMPI struggles to generate realistic textures when large missing areas exist.

View-dependent effects are important for realistic rendering, but our method cannot model view-dependent effects such as specular reflections, due to the challenge of inferring light conditions from a single image. We leave this as our future work.

6 CONCLUSION

In this paper, we proposed SinMPI, a novel single-image approach for synthesizing novel views that constructs an expanded multiplane space from a single input image, enabling fast and 3D-consistent view synthesis. Our method significantly expands the perspective range of MPIs and thus allows a wider range of camera movement. Extensive qualitative and quantitative evaluations across various datasets demonstrated that our method outperforms other state-of-the-art methods in single-image novel view synthesis.

ACKNOWLEDGMENTS

This work was supported by National Natural Science Foundation of China (Grant No.: 62372015), Center For Chinese Font Design and Research, and Key Laboratory of Intelligent Press Media Technology.

REFERENCES

- Holger Caesar, Jasper Uijlings, and Vittorio Ferrari. 2018. Coco-stuff: Thing and stuff classes in context. In *Proceedings of the IEEE conference on computer vision and pattern recognition*. 1209–1218.
- Shengqu Cai, Anton Obukhov, Dengxin Dai, and Luc Van Gool. 2022. Pix2NeRF: Unsupervised Conditional p-GAN for Single Image to Neural Radiance Fields Translation. In *Proceedings of the IEEE/CVF Conference on Computer Vision and Pattern Recognition*. 3981–3990.
- Mathilde Caron, Hugo Touvron, Ishan Misra, Hervé Jégou, Julien Mairal, Piotr Bojanowski, and Armand Joulin. 2021. Emerging properties in self-supervised vision transformers. In *Proceedings of the IEEE/CVF international conference on computer vision*. 9650–9660.
- Congyue Deng, Chiyu Jiang, Charles R Qi, Xinchen Yan, Yin Zhou, Leonidas Guibas, Dragomir Anguelov, et al. 2023. NerDi: Single-view nerf synthesis with language-guided diffusion as general image priors. In *Proceedings of the IEEE/CVF Conference on Computer Vision and Pattern Recognition*. 20637–20647.
- Jia Deng, Wei Dong, Richard Socher, Li-Jia Li, Kai Li, and Li Fei-Fei. 2009. Imagenet: A large-scale hierarchical image database. In *2009 IEEE conference on computer vision and pattern recognition*. Ieee, 248–255.
- Kangle Deng, Andrew Liu, Jun-Yan Zhu, and Deva Ramanan. 2022. Depth-supervised nerf: Fewer views and faster training for free. In *Proceedings of the IEEE/CVF Conference on Computer Vision and Pattern Recognition*. 12882–12891.
- John Flynn, Michael Broxton, Paul Debevec, Matthew DuVall, Graham Fyffe, Ryan Overbeck, Noah Snavely, and Richard Tucker. 2019. Deepview: View synthesis with learned gradient descent. In *Proceedings of the IEEE/CVF Conference on Computer Vision and Pattern Recognition*. 2367–2376.
- Chen Gao, Yichang Shih, Wei-Sheng Lai, Chia-Kai Liang, and Jia-Bin Huang. 2020. Portrait neural radiance fields from a single image. *arXiv preprint arXiv:2012.05903* (2020).
- Ian Goodfellow, Jean Pouget-Abadie, Mehdi Mirza, Bing Xu, David Warde-Farley, Sherjil Ozair, Aaron Courville, and Yoshua Bengio. 2020. Generative adversarial networks. *Commun. ACM* 63, 11 (2020), 139–144.
- Jiatao Gu, Alex Trevithick, Kai-En Lin, Joshua M Susskind, Christian Theobalt, Lingjie Liu, and Ravi Ramamoorthi. 2023. NerDiff: Single-image view synthesis with nerf-guided distillation from 3d-aware diffusion. In *International Conference on Machine Learning*. PMLR, 11808–11826.
- Yuxuan Han, Ruicheng Wang, and Jiaolong Yang. 2022. Single-View View Synthesis in the Wild with Learned Adaptive Multiplane Images. *arXiv preprint arXiv:2205.11733* (2022).
- Richard Hartley and Andrew Zisserman. 2003. *Multiple view geometry in computer vision*. Cambridge university press.
- Baichuan Huang, Hongwei Yi, Can Huang, Yijia He, Jingbin Liu, and Xiao Liu. 2021. M3VSNNet: Unsupervised multi-metric multi-view stereo network. In *2021 IEEE International Conference on Image Processing (ICIP)*. IEEE, 3163–3167.
- Ajay Jain, Matthew Tancik, and Pieter Abbeel. 2021. Putting nerf on a diet: Semantically consistent few-shot view synthesis. In *Proceedings of the IEEE/CVF International Conference on Computer Vision*. 5885–5894.
- Varun Jampani, Huiwen Chang, Kyle Sargent, Abhishek Kar, Richard Tucker, Michael Krainin, Dominik Kaeser, William T Freeman, David Salesin, Brian Curless, et al. 2021. SLIDE: Single image 3d photography with soft layering and depth-aware inpainting. In *Proceedings of the IEEE/CVF International Conference on Computer Vision*. 12518–12527.
- Rasmus Jensen, Anders Dahl, George Vogiatzis, Engin Tola, and Henrik Aanæs. 2014. Large scale multi-view stereopsis evaluation. In *Proceedings of the IEEE conference on computer vision and pattern recognition*. 406–413.
- Jiaxin Li, Zijian Feng, Qi She, Henghui Ding, Changhu Wang, and Gim Hee Lee. 2021. Mine: Towards continuous depth mpi with nerf for novel view synthesis. In *Proceedings of the IEEE/CVF International Conference on Computer Vision*. 12578–12588.
- Qinbo Li and Nima Khademi Kalantari. 2020. Synthesizing light field from a single image with variable MPI and two network fusion. *ACM Trans. Graph.* 39, 6 (2020), 229–1.
- Zhengqi Li, Qianqian Wang, Noah Snavely, and Angjoo Kanazawa. 2022. InfiniteNature-Zero: Learning Perpetual View Generation of Natural Scenes from Single Images. In *European Conference on Computer Vision*. Springer, 515–534.
- Kai-En Lin, Yen-Chen Lin, Wei-Sheng Lai, Tsung-Yi Lin, Yi-Chang Shih, and Ravi Ramamoorthi. 2023. Vision transformer for nerf-based view synthesis from a single input image. In *Proceedings of the IEEE/CVF Winter Conference on Applications of Computer Vision*. 806–815.
- Andrew Liu, Richard Tucker, Varun Jampani, Ameesh Makadia, Noah Snavely, and Angjoo Kanazawa. 2021. Infinite nature: Perpetual view generation of natural scenes from a single image. In *Proceedings of the IEEE/CVF International Conference on Computer Vision*. 14458–14467.
- Ben Mildenhall, Pratul P Srinivasan, Rodrigo Ortiz-Cayon, Nima Khademi Kalantari, Ravi Ramamoorthi, Ren Ng, and Abhishek Kar. 2019. Local light field fusion: Practical view synthesis with prescriptive sampling guidelines. *ACM Transactions on Graphics (TOG)* 38, 4 (2019), 1–14.
- Ben Mildenhall, Pratul P Srinivasan, Matthew Tancik, Jonathan T Barron, Ravi Ramamoorthi, and Ren Ng. 2021. Nerf: Representing scenes as neural radiance fields for view synthesis. *Commun. ACM* 65, 1 (2021), 99–106.
- Kamyar Nazeri, Eric Ng, Tony Joseph, Faisal Qureshi, and Mehran Ebrahimi. 2019. Edgeconnect: Structure guided image inpainting using edge prediction. In *Proceedings of the IEEE/CVF International Conference on Computer Vision Workshops*. 0–0.
- Martin E Newell, RG Newell, and Tom L Sancha. 1972. A solution to the hidden surface problem. In *Proceedings of the ACM annual conference-Volume 1*. 443–450.
- René Ranftl, Alexey Bochkovskiy, and Vladlen Koltun. 2021. Vision transformers for dense prediction. In *Proceedings of the IEEE/CVF International Conference on Computer Vision*. 12179–12188.
- Chris Rockwell, David F Fouhey, and Justin Johnson. 2021. Pixelsynth: Generating a 3d-consistent experience from a single image. In *Proceedings of the IEEE/CVF International Conference on Computer Vision*. 14104–14113.
- Robin Rombach, Andreas Blattmann, Dominik Lorenz, Patrick Esser, and Björn Ommer. 2021. High-Resolution Image Synthesis with Latent Diffusion Models. *arXiv:2112.10752* [cs.CV]
- Jonathan Shade, Steven Gortler, Li-wei He, and Richard Szeliski. 1998. Layered depth images. In *Proceedings of the 25th annual conference on Computer graphics and interactive techniques*. 231–242.
- Meng-Li Shih, Shih-Yang Su, Johannes Kopf, and Jia-Bin Huang. 2020. 3d photography using context-aware layered depth inpainting. In *Proceedings of the IEEE/CVF Conference on Computer Vision and Pattern Recognition*. 8028–8038.
- Pratul P Srinivasan, Richard Tucker, Jonathan T Barron, Ravi Ramamoorthi, Ren Ng, and Noah Snavely. 2019. Pushing the boundaries of view extrapolation with multiplane images. In *Proceedings of the IEEE/CVF Conference on Computer Vision and Pattern Recognition*. 175–184.
- Pratul P Srinivasan, Tongzhou Wang, Ashwin Sreelal, Ravi Ramamoorthi, and Ren Ng. 2017. Learning to synthesize a 4D RGBD light field from a single image. In *Proceedings of the IEEE International Conference on Computer Vision*. 2243–2251.
- Richard Szeliski and Polina Golland. 1999. Stereo matching with transparency and matting. *International Journal of Computer Vision* 32, 1 (1999), 45–61.
- Carlo Tomasi and Roberto Manduchi. 1998. Bilateral filtering for gray and color images. In *Sixth international conference on computer vision (IEEE Cat. No. 98CH36271)*. IEEE, 839–846.
- Richard Tucker and Noah Snavely. 2020. Single-view view synthesis with multiplane images. In *Proceedings of the IEEE/CVF Conference on Computer Vision and Pattern Recognition*. 551–560.
- Daniel Watson, William Chan, Ricardo Martin-Brualla, Jonathan Ho, Andrea Tagliaschi, and Mohammad Norouzi. 2022. Novel view synthesis with diffusion models. *arXiv preprint arXiv:2210.04628* (2022).
- Olivia Wiles, Georgia Gkioxari, Richard Szeliski, and Justin Johnson. 2020. Synsin: End-to-end view synthesis from a single image. In *Proceedings of the IEEE/CVF Conference on Computer Vision and Pattern Recognition*. 7467–7477.
- Suttisak Wizadwongsa, Pakkapon Phongthawee, Jiraphon Yenphraphai, and Supasorn Suwajanakorn. 2021. Nex: Real-time view synthesis with neural basis expansion. In *Proceedings of the IEEE/CVF Conference on Computer Vision and Pattern Recognition*. 8534–8543.
- Dejia Xu, Yifan Jiang, Peihao Wang, Zhiwen Fan, Humphrey Shi, and Zhangyang Wang. 2022. SinNeRF: Training Neural Radiance Fields on Complex Scenes from a Single Image. *arXiv preprint arXiv:2204.00928* (2022).
- Qiangeng Xu, Weiyue Wang, Duygu Ceylan, Radomir Mech, and Ulrich Neumann. 2019. Disn: Deep implicit surface network for high-quality single-view 3d reconstruction. *Advances in Neural Information Processing Systems* 32 (2019).
- Wei Yin, Jianming Zhang, Oliver Wang, Simon Niklaus, Long Mai, Simon Chen, and Chunhua Shen. 2021. Learning to recover 3d scene shape from a single image. In *Proceedings of the IEEE/CVF Conference on Computer Vision and Pattern Recognition*. 204–213.
- Alex Yu, Vickie Ye, Matthew Tancik, and Angjoo Kanazawa. 2021. pixelnerf: Neural radiance fields from one or few images. In *Proceedings of the IEEE/CVF Conference on Computer Vision and Pattern Recognition*. 4578–4587.
- Richard Zhang, Phillip Isola, Alexei A Efros, Eli Shechtman, and Oliver Wang. 2018. The unreasonable effectiveness of deep features as a perceptual metric. In *Proceedings of the IEEE conference on computer vision and pattern recognition*. 586–595.
- Xiaoming Zhao, Fangchang Ma, David Güera, Zhile Ren, Alexander G Schwing, and Alex Colburn. 2022. Generative multiplane images: Making a 2d gan 3d-aware. In *European Conference on Computer Vision*. Springer, 18–35.
- Bolei Zhou, Agata Lapedriza, Aditya Khosla, Aude Oliva, and Antonio Torralba. 2017a. Places: A 10 million image database for scene recognition. *IEEE transactions on pattern analysis and machine intelligence* 40, 6 (2017), 1452–1464.
- Bolei Zhou, Hang Zhao, Xavier Puig, Sanja Fidler, Adela Barriuso, and Antonio Torralba. 2017b. Scene parsing through ade20k dataset. In *Proceedings of the IEEE conference on computer vision and pattern recognition*. 633–641.
- Tinghui Zhou, Richard Tucker, John Flynn, Graham Fyffe, and Noah Snavely. 2018. Stereo magnification: Learning view synthesis using multiplane images. *arXiv preprint arXiv:1805.09817* (2018).

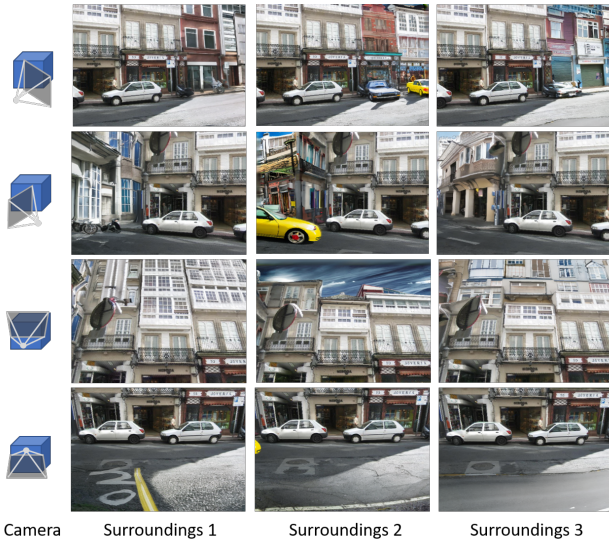


Figure 3: Single-image novel view synthesis results obtained by our SinMPI for a street scene with three different out-painted surroundings.

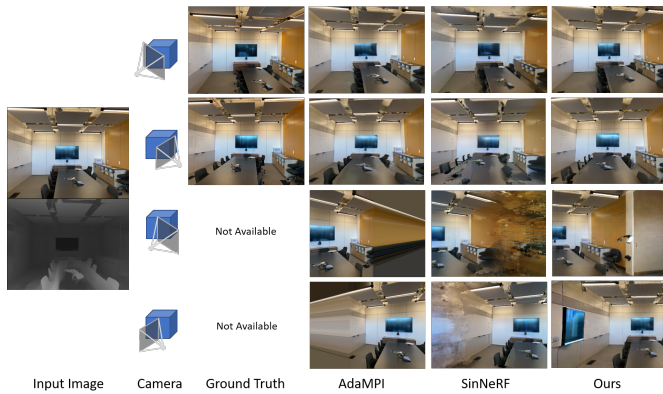


Figure 4: Qualitative results of our method against other state-of-the-art methods evaluated on the LLFF dataset (Room scene).

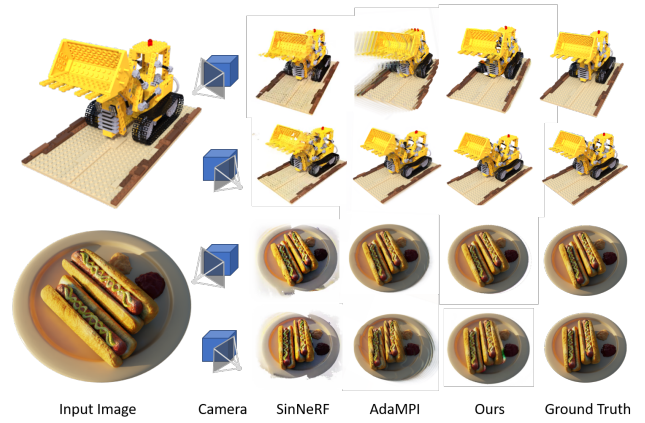


Figure 5: Qualitative results of our method against other state-of-the-art methods evaluated on the NeRF synthetic dataset (Lego scene and Hotdog scene).

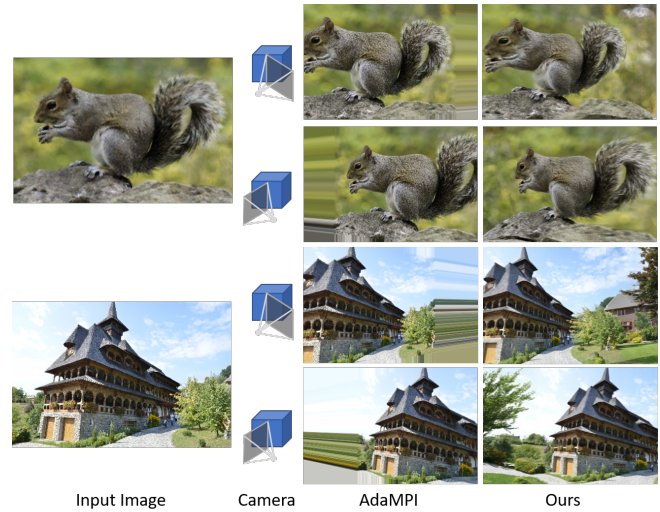


Figure 6: The demonstration of our expanded MPI supporting large camera rotation with the expanded scene. Our proposed MPI expanding strategy pushes the boundary of MPI-based methods with a larger scene capacity.

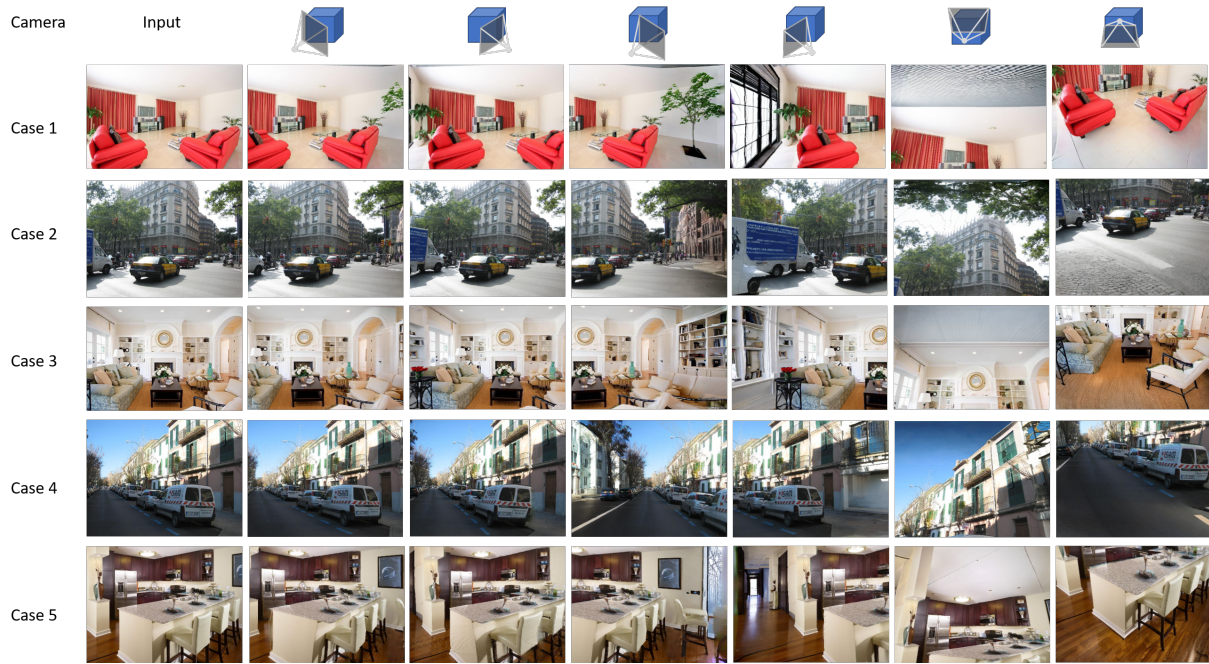


Figure 7: Single-image novel view synthesis results obtained by our SinMPI for various scenes.



Figure 8: Comparison of different inpainting approaches. Our depth-aware inpainter generates more realistic results.



Figure 9: The ablation study on DTU scan 84.